DALTON
FULL PAPER

Early photochemical dynamics of organometallic compounds studied by ultrafast time-resolved spectroscopic techniques †

Antonín Vlček Jr.,*[a] Ian R. Farrell,[a] Davina J. Liard,[a] Pavel Matousek,[b] Michael Towrie,[b] Anthony W. Parker,[b] David C. Grills[c] and Michael W. George[c]

[a] *Department of Chemistry, Queen Mary and Westfield College, University of London, Mile End Road, London, UK E1 4NS*
[b] *Central Laser Facility, CLRC Rutherford Appleton Laboratory, Chilton, Didcot, Oxfordshire, UK OX11 0QX*
[c] *School of Chemistry, University of Nottingham, University Park, Nottingham, UK NG7 2RD*

Received 13th July 2001, Accepted 11th October 2001
First published as an Advance Article on the web 22nd January 2002

Time-resolved spectroscopic techniques operating on a femtosecond–picosecond time scale are used to investigate mechanisms and dynamics of the earliest stages of photochemical reactions of organometallic compounds, as well as the composition and structure of the excited states and photointermediates involved. A deep insight into the following ultrafast photochemical reactions: (i) Cr–CO bond dissociation in $[Cr(CO)_4(bpy)]$, (ii) dissociative isomerisation of $[Mn(Br)(CO)_3(\alpha\text{-diimine})]$ and (iii) interligand electron transfer in $[Re(MQ^+)(CO)_3(dmb)]^{2+}$ has been obtained by combining time-resolved visible and IR absorption, resonance Raman and fluorescence spectroscopic techniques. In each case, it is demonstrated what kind of information individual approaches provide and how the photochemical mechanism can be deduced. The operating principles of these ultrafast spectroscopic techniques are briefly explained, together with descriptions of the experimental setups used for the above mentioned studies.

Introduction

Time-resolved absorption, fluorescence and Raman spectra, measured at very short time intervals after electronic excitation with a femto- or pico-second laser pulse provide unique information regarding the structure of electronically excited states and photochemical intermediates, as well as early photochemical dynamics. Spectral investigations, using a femtosecond–picosecond time resolution explore chemical processes which occur on the same time scale as the vibrations of chemical bonds or the reorganisation of solvent molecules.[1,2] Indeed, these are regarded as the fastest chemically relevant processes and, in this sense, ultrafast spectroscopy explores the times when chemistry really begins. Besides their fundamental importance, ultrafast photochemical dynamics have important implications for the processes of light-energy conversion, information processing by chemical means, as well as photocatalysis and photo-initiation. This is because ultrafast rates impart selectivity and directionality to photochemical processes, thereby minimising losses of energy and information. The natural processes of vision and photosynthesis clearly manifest this principle. Much of the early work into the photochemistry of transition metal complexes has focused on compounds with long-lived excited states. Such systems were believed to be optimal for converting light energy to chemical energy as well as for use in molecular devices. However, the importance and potential of complexes with short-lived excited states, which undergo ultrafast reactions, are only recently being fully appreciated.[3] For example, it was shown that electron injection from molecular sensitisers to semiconductors such as TiO_2, can occur as an ultrafast process in 25–150 fs.[4–11] This discovery removes the constraint of lifetime from sensitiser design and broadens enormously the range of potentially useful molecules, including cheap and environmentally benign iron complexes.[12] Some photoinduced electron transfer reactions in mixed-valence complexes and supramolecular systems occur on the time scale of picoseconds or even hundreds of femtoseconds,[13–16] demonstrating their potential for possible applications in optical switching and molecular electronics.[17] Other time-resolved spectroscopic studies have yielded important information concerning electron localization and initial excited state dynamics of ruthenium(II) complexes, which can serve as photosensitisers in light energy conversion systems[18–22] or as DNA intercalators.[23,24] Ultrafast photochemical reactions of organometallic compounds often generate highly reactive coordinatively unsaturated species, reactions of which can activate even C–H and C–F bonds. Femtosecond photochemical dissociation of metal–carbonyl bonds or reductive elimination of H_2 are the most common processes responsible.[25–29] Similarly, ultrafast homolysis of metal–alkyl bonds generates radicals, which can initiate polymerisation.[30] Other, presumably ultrafast, photochemical metal–ligand bond splitting reactions produce solvated Lewis-acidic metal cations or strongly basic free ligands which can also act as polymerisation initiators.[30–32] Several mechanistic studies of ultrafast organometallic photochemical reactions have indicated that their final outcome (*i.e.* selectivity, yield and nature of the products) is often dictated by the dynamics of the excited state(s) involved at the very earliest times after excitation.[33–37] Consequently, ultrafast spectroscopic studies have great potential to provide a fundamentally new understanding of organometallic reactions on the fastest possible time scales. Furthermore, they are a source of enabling knowledge for light-energy conversion, molecular electronics and photonics, as well as for photocatalysis and photoinitiation.

Ultrafast time-resolved (TR) spectroscopy has undergone a revolution during the 1990's, brought about by the advent of femtosecond titanium sapphire, Ti : S, lasers and regenerative amplifiers stemming from the discovery of Kerr-lens modelocking.[38] The extremely broad fluorescence bandwidth of the Ti : S gain medium enables the generation of femtosecond or

† Based on the presentation given at Dalton Discussion No. 4, 10–13th January 2002, Kloster Banz, Germany.

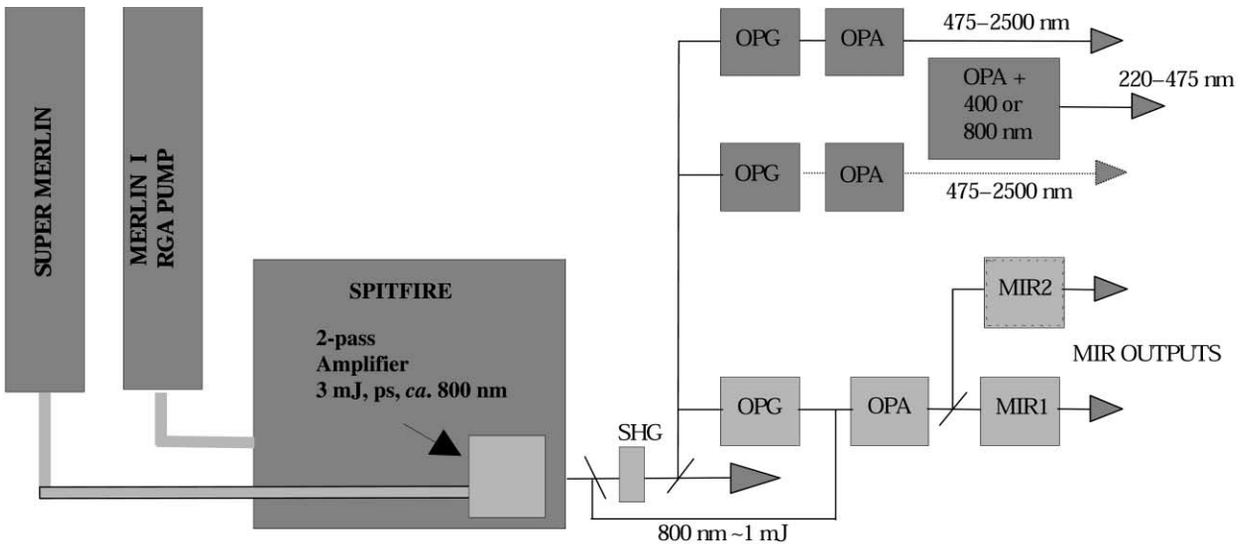

Fig. 1 Multicolour pump and probe ultrafast laser source. Two Merlin Nd : YLF lasers pump a SuperSpitfire titanium sapphire system amplifying pulses derived from a Ti : Sapphire oscillator (Tsunami). The amplifier generates pulses of either 150 fs or 1–3 ps pulse length and *ca.* 2 mJ energy at a 1 kHz repetition rate. This output then pumps OPAs to deliver synchronised outputs of any colour. Ultraviolet and mid-infrared outputs are created by further frequency up or down conversion in non-linear crystals.

picosecond laser pulses at about 800 nm. These lasers are now commercially available, and are stable and robust enough to be used in chemical laboratories. The availability of both the high pulse energies and short pulse durations makes these lasers and amplifiers an ideal pump source for optical parametric generators (OPG) and optical parametric amplifiers (OPA) facilitating, in combination with upconversion and downconversion, a relatively easy access to an extremely broad range of wavelengths (200–10,000 nm).[39] A single Ti : S laser/regenerative amplifier can simultaneously pump two or more independent OPAs. Additionally, higher pulse energies are available at 400, 267 or 200 nm *via* high harmonic generation from the 800 nm Ti : S fundamental and these can also be used directly for spectroscopic experiments or combined with an OPA output. Such a multicolour laser light source (Fig. 1) produces two or more trains of fs or ps pulses, the wavelength of each being independently tuneable throughout the visible and IR spectral regions (the UV region is accessible by frequency doubling or mixing). Ultrashort pulses of white light continuum can also be generated by passing the 800 nm femtosecond fundamental Ti : S laser pulses through materials such as D_2O, sapphire or CaF_2. It is important to note that the various laser beams of different colours produced in this spectroscopic laser source are derived from a single Ti : S pump laser. Hence, they are perfectly temporally synchronized and the relative timing of their arrival at the sample can be controlled by changing optical path lengths using motorized delay lines. The simultaneous availability of two independently tuneable, synchronized ultrafast laser pulses (Fig. 1) allows us to perform various kinds of "pump–probe" time-resolved spectroscopic experiments: The sample is excited with one laser pulse (pump) and its spectroscopic properties studied by another laser pulse (probe), which arrives after a known, controllable, time-delay, Fig. 2. Alternatively, pulses of a white light continuum can be used as a probe beam for experiments where a broad spectral region is explored.

It is convenient to begin mechanistic investigations of ultrafast photochemistry with time-resolved visible absorption spectroscopy. Present techniques using white light continuum probe pulses and multichannel detection allow us to measure visible absorption spectra at selected time delays after excitation. Analysis of the evolution of the spectrum yields precise kinetic information, from tens of femtoseconds upwards, and reveals the presence of excited states and photointermediates and the number of reaction steps involved. Time-resolved experiments in the UV spectral region are more complicated

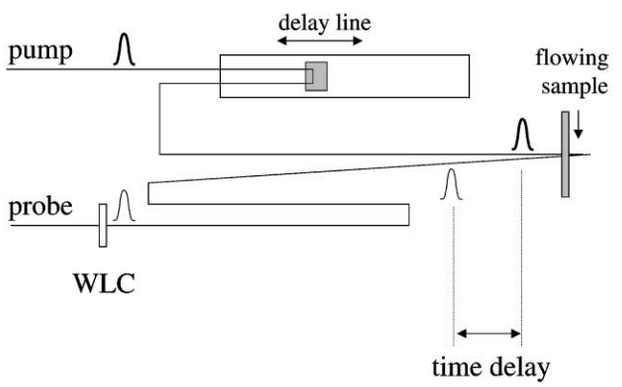

Fig. 2 General principle of pump–probe femtosecond–picosecond time-resolved spectroscopy. A short pump pulse is used to excite a small portion of the sample. A snapshot of the reactions of the excited species and formation of products is taken using a probe pulse which arrives delayed in time. The time delay between the pump and probe is precisely controlled using an optical delay line. For example a 0.15 mm movement of the delay line corresponds to changing the pump–probe timing by 1 ps. Delays of up to 6 ns are possible on the system described. White light continuum, WLC, probe is used for time-resolved visible absorption. IR absorption spectroscopy uses broad-band IR pulses, whereas probe pulses for TR^3 have to be spectrally as narrow as possible at a given pulse duration, see the text.

because of the technical difficulties associated with generation of ultrafast pulses of UV spectral continuum. Nevertheless, it is possible to study the time-dependence of absorbance at a single UV wavelength.

Although time-resolved UV-Vis absorption spectroscopy provides excellent kinetic data, the amount of structural information on photochemical intermediates it yields is rather limited. It can sometimes be difficult to distinguish excited states from primary photoproducts. This problem can be addressed using time-resolved vibrational spectroscopy, namely IR absorption and resonance Raman. These two techniques are complementary, often specific for different groups of vibrational modes within a molecule. For example, frequency shifts of marker vibrations, such as ν(CO) in metal carbonyls or ν(CN) in α-diimines or polypyridines, upon excitation are especially useful in excited state characterization. Whilst ν(CO) vibrations are strongly IR-active, the α-diimine ν(CN) modes are much more visible in resonance Raman spectra. The Raman technique is particularly useful for studying modes in the

fingerprint region of chemical and biological systems in aqueous or other IR-absorbing solvents. Resonance Raman provides additional specificity through the resonance enhancement effect that increases, by up to five orders of magnitude, the Raman scattering of the particular molecule or chromophore that absorbs light at around the wavelength of the probe beam. IR absorption bands and Raman peaks often show time-dependent shifts and line-broadening on the femto–picosecond time scale, analysis of which yields important information concerning vibrational relaxation. Another important technique is time-resolved fluorescence, which is only rarely studied on picosecond or shorter time scales. Nevertheless, a comparison of absorption and fluorescence dynamics can easily distinguish excited states from primary photochemical products, while time-dependent fluorescence spectral shifts reveal details of vibrational relaxation and/or solvation dynamics.

A full mechanistic understanding of ultrafast photochemical reactions is provided by comprehensive studies based on a combination of the different femto–picosecond time-resolved (TR) spectroscopic techniques mentioned above. In an ideal case, we should proceed from a detailed study of reaction dynamics by TR-UV-Vis absorption to structure-sensitive techniques such as TR-IR absorption of resonance Raman, complemented with TR emission. In this article, we will illustrate the power of this comprehensive approach by discussing mechanistic studies of the following ultrafast organometallic photoreactions: (i) Cr–CO bond dissociation in $[Cr(CO)_4(bpy)]$, (ii) dissociative isomerisation of $[Mn(Br)(CO)_3(\alpha\text{-diimine})]$ and (iii) interligand electron transfer in $[Re(MQ^+)(CO)_3(dmb)]^{2+}$. These reactions represent some typical photoprocesses of charge transfer excited states of organometallic compounds, namely photofragmentation, molecular rearrangement and intramolecular electron transfer. Their mechanisms and dynamics were studied using the unique combination of time-resolved spectroscopic techniques developed at the Ultrafast Spectroscopy Laboratory of the Rutherford Appleton Laboratory. The technical aspects of this state-of-the-art equipment will be briefly summarised.

Experimental

The experiments discussed herein have been carried out using the equipment available at the Ultrafast Spectroscopy Laboratory of the Central Laser Facility, CLRC Rutherford Appleton Laboratory (RAL). This equipment is designed for studying transient species on the picosecond time scale. A laser pulse length of ≈200 fs, 1 ps or 2–3 ps can be selected. The fastest overall instrument time resolution attainable at the time of writing is *ca.* 400 fs.

General considerations

The general principle of ultrafast pump–probe techniques was briefly outlined in the Introduction. They rely on the creation of transient species in sufficient concentration to be detected by transient absorption, fluorescence or Raman spectroscopy. The strength of the transient signal is dependent on many parameters such as the molar absorptivity of the sample molecules in their ground and photo-product states, the laser intensity and the geometry of the light-collection system. A laser system operating with a *ca.* 1 kHz repetition rate offers a good compromise between the requirements for pulses of sufficient energy and average power to detect transient species, while allowing pump and probe geometries that minimise unwanted non-linear effects. Therefore, by design, a very wide range of samples can be studied. For example the experiment can be tailored by reducing pump or probe powers to avoid saturation of molecular transitions with large molecular absorptivities or by designing sensitive detection techniques that enable weakly absorbing molecules or species in low concentrations to be studied, while avoiding non-linear effects. The relative orientation of polarisation directions of pump and probe pulses is another factor to be considered. All time-resolved absorption and emission experiments described herein were performed using a magic angle (54.7°) orientation, in order to avoid any effects due to anisotropy. However, rotation dynamics of excited or photoproduct molecules, which occur on the time scale of tens of picoseconds, can be followed using parallel or perpendicular relative polarisations.[35,40] Time-dependent polarisation effects have been, for example, employed to study electron-localization in $[M(bpy)_3]^{2+}$ ($M = Ru^{II}$, Os^{II}) complexes.[19,41]

For ultrafast spectroscopy, a short sample thickness is desirable. This helps to reduce the transit-time spread of the pump and probe pulses and, in particular for Raman spectroscopy, optimises light collection. The concentrations of the samples are typically adjusted to give an absorbance of between 0.5 and 1.0 in a 1 mm optical path-length at the wavelength of the pump laser. In order to avoid secondary photochemistry and excessive heating, the sample solution is circulated through the cell. However, the sample solution is static at the interface between the solution and a cell window. Hence, degradation caused by 'burning' of the sample is often encountered, especially in studying irreversible photochemical reactions such as fragmentation. This is often manifested by the deposition of a dark solid material at the cell window, which spoils the experiments. Measuring spectra from an open jet solution (200 μm–1 mm diameter) solves this problem.

Multicolour pump and probe laser source

The dual OPA amplifier concept, first pioneered in the development of TR^3 spectroscopy at RAL, proved to be an ideal choice for providing independently tuneable, high-energy pulses synchronised on a pico–femtosecond time scale.[42–44] This system was designed for fs and ps pump and probe time-resolved absorption and Raman spectroscopy. The layout of the dual OPA system is shown in Fig. 1. The pump laser is a Ti : S regenerative amplifier (Spectra-Physics/Positive Light, Super-Spitfire) seeded by a ≈100 fs pulse, generated by a self mode-locked Ti : S laser (Spectra-Physics, Tsunami). The Ti : S regenerative amplifier operates in two modes, picosecond or femtosecond, at a 1 kHz repetition rate, delivering *ca.* 800 nm pulses, with an energy of 2–3 mJ per pulse. The picosecond mode delivers output pulses that can be varied between *ca.* 1 and 2–3 ps pulse duration resulting in *ca.* 15 to 7 cm^{-1} bandwidth, respectively. The pulses are frequency doubled and split to pump two optical parametric amplifiers (OPA) seeded using spectrally filtered optical parametric generators (OPG) to deliver 1 ps pulses with ≈35 cm^{-1} bandwidth (or optionally 2–3 ps with 10–15 cm^{-1}) of ≈10 μJ pulse energy across the tuning range of 460–700 nm. In the femtosecond mode, the regenerative amplifier gives an output pulse of 150 fs duration and 100 cm^{-1} bandwidth. With 150 fs pump pulses, the OPAs can be reconfigured to deliver ≈200 fs pulses of ≈10 μJ pulse energy. Combined with upconversion and including the idler tuneability the overall tuning range is 205–2800 nm. Moreover, the Ti : S laser can also pump OPAs operating in the mid-infrared spectral region (MIR). This facility is used to generate an IR probe beam in the case of TR-IR spectroscopy (PIRATE), which is described in more detail below. Alternatively, the OPAs can be bypassed and the output of the Ti : S amplifier is then used directly. This option is employed especially in the following cases: (i) pumping the sample at 400 nm using the second harmonic of the Ti : S fundamental or at 267 nm which is obtained by mixing of 400 and 800 nm Ti : S beams; (ii) using the 800 nm fundamental to generate[45–47] a white light continuum, WLC, probe beam for spectrally broadband studies and (iii) generation of the Raman probe beam at either 400 or 267 nm. All the light beams produced by this lasers source, including the WLC are linearly polarised.

Time-resolved visible absorption

The transient absorption system (Fig. 2) uses short, *ca.* 200 fs, pump pulses, that are tuneable from 205 nm in the ultraviolet through to 2800 nm in the near-IR region, and very broadband white-light continuum probe pulses, WLC, of a comparable duration, which are generated by a small portion of the 800 nm Ti : S beam focused in water. The pump and probe beams propagate nearly collinearly and overlap in the sample over an area of *ca.* 200 μm in diameter. A dual diode array arrangement simultaneously monitors the dispersed spectrum from a probe pulse that travels through the excited sample and a reference that is split from the probe before the sample, Fig. 3. The dual

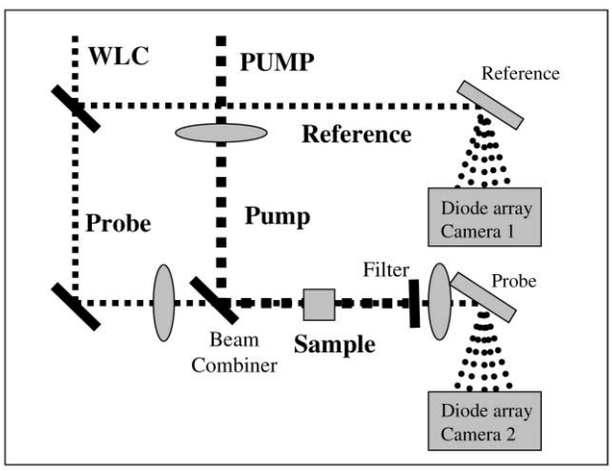

Fig. 3 Detection system used in time-resolved visible absorption spectroscopy. The "white" probe beam (WLC) is split by a 50/50 beamsplitter to provide probe and reference beams. Two gratings disperse the spectrum between *ca.* 420 and 720 nm onto the diode arrays. The spectra are recorded and normalised shot by shot. The sample is inserted in the probe line where transient species are created with a pump laser. The reference beam by-passes the sample.

camera system was custom-built by Cronin Electronics. Each array consists of 512 elements with a sensitive area of 25 by 2 mm. Fast electronics enable real time readout and analysis of the array signal in a standard PC. A shot-by-shot normalisation reduces the influence of fluctuation in the laser pulse energy. The instrument operates with the following specifications: Difference absorbance sensitivity of less than 10^{-3} is typically achieved in ten minutes of data accumulation at a maximum repetition rate of 0.8 kHz. The instrument response time is *ca.* 400 fs. The current probe wavelength range is 420–770 nm. The output is presented in the form of difference absorption (ΔA) spectra whereby the spectrum measured before excitation is subtracted from the spectrum measured at a given time after excitation. Absorption bands due to photogenerated species are thus positive and those which correspond to the depleted ground state are negative, referred to as bleach. Time-resolved visible spectra measured at time delays shorter than 2–3 ps are distorted by the, so called, spectral chirp which is due to light dispersion in transparent materials, such as the medium in which the WLC is generated, cell windows and the sample itself. Different spectral components of the WLC propagate through these media with different velocities. The red part of the WLC then arrives earlier at the sample relative to the blue part by up to *ca.* 1.5 ps. This affects the relative timing of the arrival of pump and probe beams at the sample. As a result, we see a progressive shift in the apparent position of transient absorption bands from blue to the red as the time delay increases from 0 to 2–3 ps.

Further improvement of the current configuration is under way, especially with regards to a faster readout and analysis to enable greater signal discrimination. The use of a shorter pulse 'single filament' white light continuum will increase instrument response, provide greater tuning range and increase sensitivity.

Picosecond infrared absorption and transient excitation (PIRATE)

The time-resolved infrared absorption spectrometer is based on the general concept of pump–probe spectroscopy, shown in Fig. 2. An IR probe beam is used instead of WLC. Since vibrational transitions are generally much weaker than electronic transitions, an ability to observe very small absorbance changes, down to 10^{-4}–10^{-5} or better, is desirable. This high sensitivity requires a high quality time-resolved spectrometer apparatus. This was achieved at RAL by using a combination of stable optical parametric amplifiers and difference frequency generators, a dual infrared diode-array for referencing and shot-by-shot discrimination by the software.[48]

The Ultrafast Spectroscopy Laboratory at RAL uses difference frequency generation[49–55] in non-linear materials such as silver gallium sulfide, $AgGaS_2$, to provide IR probe pulses in the 'fingerprint' region 1000–3000 cm^{-1}. The width of the infrared output may be either: (i) *ca.* 200 fs broad-band, which corresponds to a wavenumber range of 150–200 cm^{-1} or (ii) 1 ps narrow-band, *ca.* 25 cm^{-1}. The broad-band output is useful for spectrally dispersed time-resolved IR absorption studies while the latter is employed for experiments that require pumping or probing of specific IR-active modes. Pulse energies of several μJ at 1 kHz repetition rate are easily attainable.

The dual diode-array system at RAL[48] comprises of two Infrared Associates Inc. MCT-13-64el arrays of 64 elements each. It allows the simultaneous measurement of the spectra of broadband infrared reference and probe beams which travel by similar optical paths through two spectrometers where the beams are spectrally dispersed onto the arrays. All 128 signals from the arrays are pre-amplified (MCT-64000 Infrared Systems Development Corp.) and then captured by a custom-designed sample and hold analogue multiplexer system, the HX2, designed at the Rutherford Appleton Laboratory, before being read into a Datel 416J analogue to digital convertor card inside a standard 500 MHz personal computer. The data are analysed in pump on/pump off pairs at 1 kHz to create a rolling average using the following equation:

$$\Delta A_N = \log[1 + I_R/I_P((I_{probe}/I_{ref})_{pump\ on} - (I_{probe}/I_{ref})_{pump\ off})] + \Delta A_{N-1}(N-1)/N \quad (1)$$

where I_R and I_P are the final averages of the 'pump off' spectra on the reference and probe sides, respectively and N is the number of acquisitions. The reference is used to normalise pulse-to-pulse instabilities in the IR system. In contrast to the visible transient absorption apparatus, data acquisition from this IR detection system is fast enough to allow shot-by-shot discrimination at 1 kHz. This removes large signal fluctuations induced by laser 'drop outs' or other large variations such as those associated with gas bubbles in the sample flow stream.

The pump and infrared probe beams are focused to less than 200 μm diameter in a flowing sample. The sample can be either in a form of open jet (typically of 1 mm diameter) or an enclosed optical cell (10–1000 μm). Thin cells are used for probing of samples in aqueous solutions, *e.g.* biological samples. For probing below 1700 cm^{-1}, N_2-purged 'dry' infrared beam paths are used to reduce probe beam absorption by water vapour in the air. 'Burning' of the sample at the cell windows, as mentioned above, can be further reduced by a rastering movement of the flow cell. All-infrared optical elements are based on gold reflective optics or CaF_2. Operation at wavelengths >8 μm would require replacing CaF_2 with ZnSe or reflective optics. The current configuration allows probing from 2 to 8 μm (*i.e.* 5000–1250 cm^{-1}) and pumping anywhere between 205 and 2800

nm. The system is capable of detecting changes in absorbance of $\Delta A < 10^{-3}$ in a 1 second accumulation at 1 kHz repetition rate, with an instrument response of ≈400 fs and ≈200 cm^{-1} spectral coverage. If required, the probe range can be expanded to 1–15 μm (*i.e.* 10,000–670 cm^{-1}), thereby allowing the lower wavelength detection limit of the infrared spectrometer to overlap with the upper wavelength region of the silicon detector system.

Time-resolved resonance Raman (TR^3)

Time-resolved resonance Raman (TR^3) spectroscopy is complementary to the more conventional transient absorption, gain and fluorescence spectroscopies used in studying ultrafast phenomena. However, unlike these techniques, TR^3 enables the vibrations of photogenerated molecules to be probed. The experiment yields both structural and kinetic information about the intermediates created immediately after photoexcitation of solutions and solids.

As a technique, TR^3 has the power to study the processes of intramolecular vibrational relaxation, solvent relaxation/reorganisation and electron transfer, all of which manifest themselves through ultrafast changes in molecular vibrations. TR^3 belongs to the "pump and probe" family of techniques (Fig. 2) which is based on generating transient species with a picosecond pump laser pulse and obtaining their Raman spectrum using a second, time delayed, monochromatic picosecond pulse (probe). The wavelength of the latter has to be tuned into the absorption band of the investigated photogenerated species, in order to achieve resonance enhancement of Raman scattering. Hence, it is desirable to measure the time-resolved absorption spectrum in the visible spectral region prior to TR^3 experiments. The availability of an easily tuneable, multicolour photoexcitation laser source that allows the independent selection of the pump and probe wavelengths (*vide supra*) is an essential requirement for a ps-TR^3 spectrometer.[44]

The quality of ps-TR^3 spectra is dictated by a balance of many factors. The laser system should provide several mW of average power, for both pump and probe beams. A high repetition rate (≈1 kHz) is needed and the pump and probe beams have to be synchronised temporally to within <200 fs of each other. Additionally, high spectral brightness, and the ability to tune the wavelength of the pump and probe beams continuously from the UV to the near-IR, where most molecular systems have electronic absorption bands, are important. The apparatus parameters are also dictated by other important experimental considerations, such as: the sample volume in which the pump and probe beams overlap; the speed of the sample solution flow (*i.e.* fresh sample must be provided for each pair of pump and probe pulses), the molar absorptivities of the ground state and the transient species, the Raman cross-section of the transient species, the minimal fluorescence and re-absorption of the Raman scattered light and the efficiency of the scattered-light collection (*e.g.* spectrometer slit size, magnification and the *f*-number of the collection optics).

Fluorescence is perhaps the single most limiting factor in ps-TR^3 spectroscopy. In many cases the pump and/or probe beams can induce fluorescence from the sample itself, contaminants or the solvent. Fluorescence can easily swamp the weak Raman scattered light thus limiting observations to particularly strong Raman bands. To address this problem, some of the authors have developed[56,57] a unique system, comprising of a fast (4 ps) optical shutter—the "Kerr gate" (K-TR^3). This enables the separation of fluorescence from Raman scattering in the time domain, using the main distinguishing feature of the Raman scattering, that is its promptness. A short-pulsed Raman signal is generated using a ps laser probe pulse. The gate is opened by another, intense ps pulse only for the passage of this Raman signal and closed immediately afterwards. The longer-lived fluorescence is thus rejected.

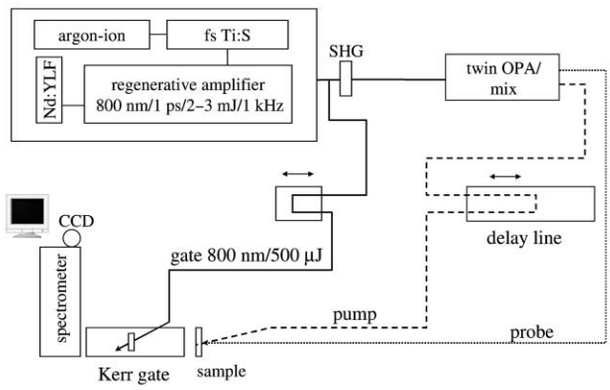

Fig. 4 Layout of the picosecond time-resolved resonance Raman (TR^3) spectrometer with the Kerr gate facility. See the text for explanation.

The layout of the instrument used herein is shown in Fig. 4. Raman scattering from a sample solution (flowed as a 500 μm diameter open jet) is excited by the probe pulse[44] arriving at the sample after the pump beam at a delay time determined by an optical delay line. The Raman signal is collected at 90° with respect to the probe beam propagation direction. The Raman light then passes through the Kerr gate and is imaged at the entrance slit of a Triplemate triple spectrograph. The spectrally dispersed Raman light is then directed at a Jobin Yvon 2000 × 800 pixel back-illuminated CCD detector cooled by liquid nitrogen. To enhance the overall throughput of the system, a home built by-pass option for the first two stages of the Triplemate spectrometer is used in spectral regions where holographic supernotch filters are available to reject intense Rayleigh scattering from entering the final dispersive stage. Data collection is accomplished by opening the CCD shutter for, typically, 10–20 seconds and acquiring all photons reaching it during this 'acquisition time'. This is repeated 10–20 times to average-out any random noise. The signal is collected at different time delays by randomly 'jumping' from one delay to another. The complete pattern of time delays is stepped through 5 or 10 times to average out all potential systematic signal fluctuations. Parallel orientation of the polarisation directions of the pump and probe pulses is usually used. The wavenumber resolutions are *ca.* 35 and 15–10 cm^{-1}, for 1 ps and 2–3 ps modes, respectively. The Kerr gate has a transmittance, in its open state, up to 40%; a rejection ratio in the closed state of 10^{-5} and a usable spectral range of 300–700 nm.

The Kerr gate[56] is incorporated within the Raman collection system and consists of two crossed polarisers and a Kerr medium (CS_2 or benzene), see Fig. 5. In the closed state, light

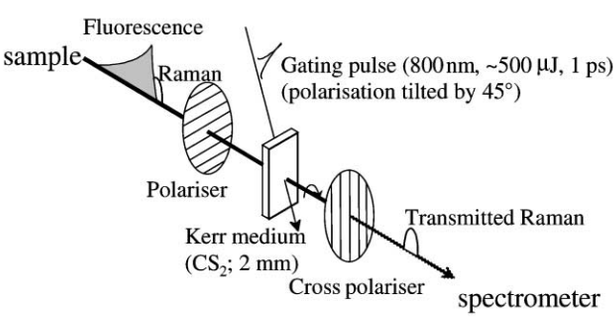

Fig. 5 Principle of the 4 ps Kerr gate used in TR^3 and time-resolved fluorescence spectroscopy. See the text for explanation.

such as fluorescence is effectively blocked by the polarisers. An intense, short gating pulse (Ti : S fundamental at 800 nm) with polarisation tilted by 45° arrives at an angle of *ca.* 10° relative to the optical axis. It creates a transient anisotropy within the Kerr medium by the optical Kerr effect. The intensity of the gating

pulse is chosen to make the medium act as a $\lambda/2$ waveplate and rotate the polarisation of any passing light, such as the instantaneous Raman signal, by 90°, thereby allowing it to be transmitted through the cross polariser. When the main fluorescence flux arrives later, after the anisotropy of the Kerr medium has decayed and gate closed, it is effectively blocked by the second polariser.

Kerr gate emission

The ps Kerr gate TR^3 spectrometer can be rapidly converted into a set-up for measuring ps time-resolved fluorescence. This is accomplished by blocking the probe pulse and replacing the Raman spectrometer grating with a low-density one (100 groves mm^{-1}) to enable wide spectral-coverage fluorescence measurements. The resulting time resolution is 4 ps. A further development of this system to provide a ≈200 fs overall resolution is planned.

Materials

The synthesis, characterization and handling of the complexes studied have been described elsewhere.[35,58,59] Details of the particular ultrafast spectroscopic experiments are summarised in the corresponding figure captions.

Results and discussion

Photodissociation of an axial CO ligand from [Cr(CO)$_4$(bpy)]: application of quantum yield measurements and ultrafast time-resolved visible and IR absorption spectroscopy

Irradiation of [Cr(CO)$_4$(bpy)] with visible light excites a Cr⟶bpy metal to ligand charge transfer (MLCT) electronic transition, triggering dissociation of an axial CO ligand.[35,60–65] The CO-loss intermediate coordinates a solvent molecule to produce *fac*-[Cr(L)(CO)$_3$(bpy)] as the only photoproduct (L = solvent or a Lewis base molecule, *e.g.* phosphine):

$$[Cr(CO)_4(bpy)] \xrightarrow{h\nu, L} fac\text{-}[Cr(L)(CO)_3(bpy)] \qquad (2)$$

The photochemical quantum yield of reaction (2) was measured[64] in several solvents as a function of excitation wavelength and temperature using the monochromatised light of a Xe-lamp. Double-beam detection of absorbed light intensity and correction for light absorption of the photoproduct were employed. The ligand PPh_3 was present in a large excess to ensure that all CO-loss species were converted into the final photoproduct *fac*-[Cr(PPh_3)(CO)$_3$(bpy)]. It was found[64] that the quantum yield of CO loss decreases as the irradiation wavelength increases over the region of the MLCT absorption band. This finding indicates that the reacting excited state keeps a "memory" of the original excitation energy. In other words, CO dissociation has to occur directly from the Franck–Condon excited state, prior to any energy relaxation or thermalization. Moreover, the photochemical quantum yield was found to be temperature-dependent, the apparent activation barrier increasing with the excitation wavelength. Similarly, pressure-dependent studies of the quantum yield of photochemical CO substitution of [Cr(CO)$_4$(phen)] have shown that reaction (2) occurs with a positive volume of activation, which increases with decreasing irradiation wavelength.[61–63] All these results show the high value of relatively simple photochemical experiments which, using continuous irradiation, can provide useful information regarding the nature of primary photochemical steps and even imply their ultrafast character. However, a detailed understanding of the excited state dynamics responsible for the photoreactivity and identification of photochemical intermediates requires the use of ultrafast time-resolved spectroscopic techniques.

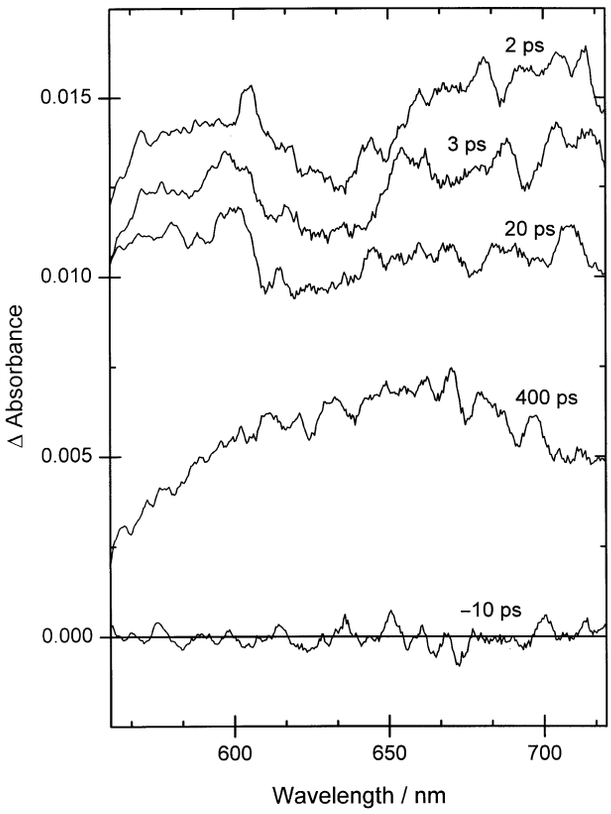

Fig. 6 Time-resolved visible absorption spectra of [Cr(CO)$_4$(bpy)] in pyridine solution, recorded at various time-delays after 500 nm, ≈200 fs (FWHM) excitation. The spectra were measured with pulses of white light continuum used as a probe beam.[35] The −10 ps spectrum shows the baseline, measured 10 ps before excitation. Five-point adjacent averaging was applied to smooth the data.

Shown in Fig. 6 are visible absorption spectra of [Cr(CO)$_4$(bpy)] in pyridine solution, measured at selected times after 250 fs, 400 nm excitation pulse. The early spectra, measured at time delays between 3 and 50 ps show a very broad absorption which evolves over the next *ca.* 100 ps into a single broad band, centred at 640 nm, whose shape and intensity does not change further. This final band was attributed to the photoproduct *fac*-[Cr(L)(CO)$_3$(bpy)] (L = py), by comparison with nanosecond TR-UV-Vis and IR spectra recorded earlier.[65] The rapidly decaying absorption seen at early times appears to be composed of the 640 nm band, which is due to *fac*-[Cr(L)(CO)$_3$(bpy)], and another broad absorption, which extends deep into the red spectral region. This is typical of the bpy$^{\bullet-}$ chromophore[66] which is present in Cr⟶bpy MLCT excited states, which can be formally viewed as [Cr$^{\mathrm{I}}$(CO)$_4$(bpy$^{\bullet-}$)].

Detailed kinetics of spectral evolution, on the femto- and pico-second time scales, were studied at various probe wavelengths and as a function of the excitation (pump) wavelength. It was found that the observed rate of the rise in transient absorption after laser pulse excitation is instrument-limited. Hence, all the transients are formed within 400 fs of excitation, which is the instrument time-resolution. Further dynamic information was obtained on the picosecond time scale.

Regardless of the pump and probe wavelength, the decay in transient absorption (Fig. 7) follows biexponential kinetics (3) with two time-constants: $\tau_1 = 8 \pm 1$ and $\tau_2 = 87 \pm 3$ ps.[35] This biexponential decay was attributed to the decay of two MLCT states, which are responsible for the initial broad absorption shown in Fig. 6. The absorption due to the photoproduct is assumed to be constant on the time scale investigated, being described in eqn. (3) by the term A_0.

To summarise, time-resolved visible absorption spectroscopy indicates that optical excitation of [Cr(CO)$_4$(bpy)] into its

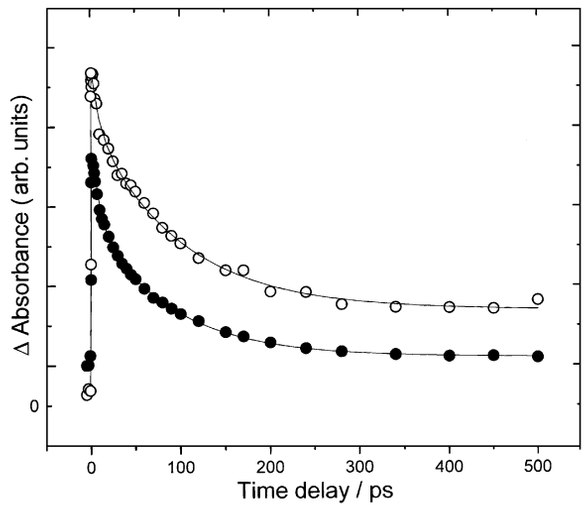

Fig. 7 Typical kinetic profiles of the differential absorbance ΔA over time, following 500 nm, ≈200 fs (FWHM) excitation of $[Cr(CO)_4(bpy)]$ in pyridine solution. Monitoring wavelengths (○ = 640 nm; ● = 800 nm) were selected from the white-light continuum probe pulse using 10 nm band-pass interference filters. Detection was performed by two (sample, reference) photodiodes. The pump beam was mechanically modulated and the absorption-induced modulation in the signal detected by a lock-in amplifier. This mode of "single wavelength" measurement is described in ref. 35. The solid lines superimposed over the data points represent non-linear curve-fits of eqn. (3) to the data. In both cases, R^2 was found to be in excess of 0.99 and very little or no systematic residuals were observed.

$$A(t) = A_0 + A_1 \exp\left(-\frac{t}{\tau_1}\right) + A_2 \exp\left(-\frac{t}{\tau_2}\right) \qquad (3)$$

^{1}MLCT excited state is followed by ultrafast CO dissociation, which occurs alongside relaxation into two lower-lying excited states, presumably ^{3}MLCT, which then decay to the ground state with lifetimes of 8 and 87 ps. They behave as "trapping states", whose population prevents CO dissociation. This mechanism is shown in Scheme 1. Provided that this interpretation is correct, the term $A_0/(A_0 + A_1 + A_2)$ reflects the branching ratio between the reaction and relaxation pathways and should depend on the excitation wavelength in the same way as the quantum yield. Indeed, this dependence has been observed, thereby demonstrating the relationship between the ultrafast excited state dynamics and overall photochemistry.[35]

Despite all of its successes, the fs–ps time-resolved visible absorption study of reaction (2) leaves several questions open. It should also be noted that most of the mechanistic information was inferred from kinetics. The assignment of the 640 nm absorption band to the *fac*-$[Cr(L)(CO)_3(bpy)]$ photoproduct is only indirect, based on comparison with a previous nanosecond time-resolved study[65] and an assumption that no chemical reactions or structural changes occur between *ca.* 500 ps and 10 ns. The particular isomeric form of the primary photoproduct (facial or meridional) thus cannot be determined unequivocally. Additionally, the description of the trapping states as ^{3}MLCT is tentative, deduced solely from the very broad, unresolved shape of the absorption band measured at 3 ps and from structural considerations. The negative absorption due to the bleached ground-state population and the positive absorption due to transient formation overlap to a great extent and the kinetic behaviour of the individual species cannot be discerned. Hence, TR visible absorption spectroscopy does not prove directly that the ground state of $[Cr(CO)_4(bpy)]$ reforms during the decay of the ^{3}MLCT states. Furthermore, the kinetic data do not discard the possibility that the ^{3}MLCT states themselves undergo CO dissociation, resulting in $[Cr(L)(CO)_3(bpy)]$ formation. These issues can only be addressed using picosecond time-resolved IR absorption spectroscopy.

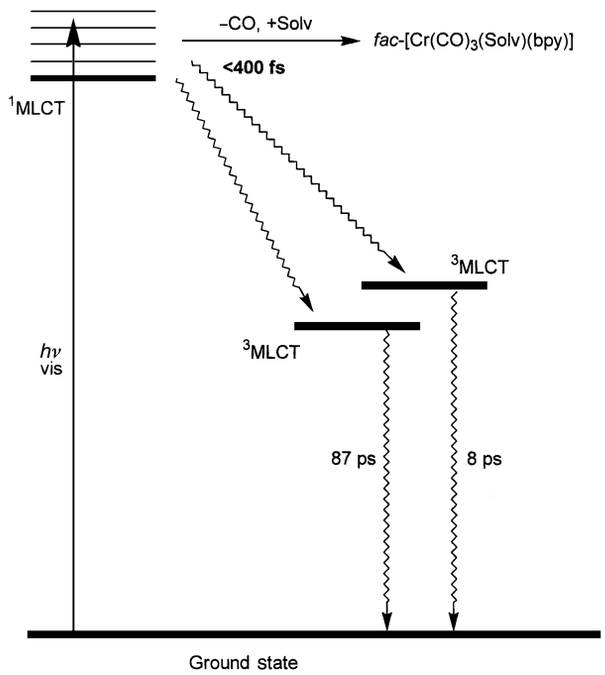

Scheme 1 Excited state dynamics and photochemistry of $[Cr(CO)_4(bpy)]$. Excitation with a fs pulse of a visible light prepares a ^{1}MLCT Franck–Condon excited state which undergoes either ultrafast CO dissociation or relaxation into lower-lying ^{3}MLCT states. This branching of Franck–Condon excited-state evolution between reactive and relaxation pathways is completed within 400 fs. The photochemical quantum yield is determined by the corresponding branching ratio, which depends on the initially populated vibronic level, that is on the excitation wavelength. The ^{3}MLCT states are unreactive, decaying directly to the ground state with lifetimes of 8 and 87 ps, respectively.

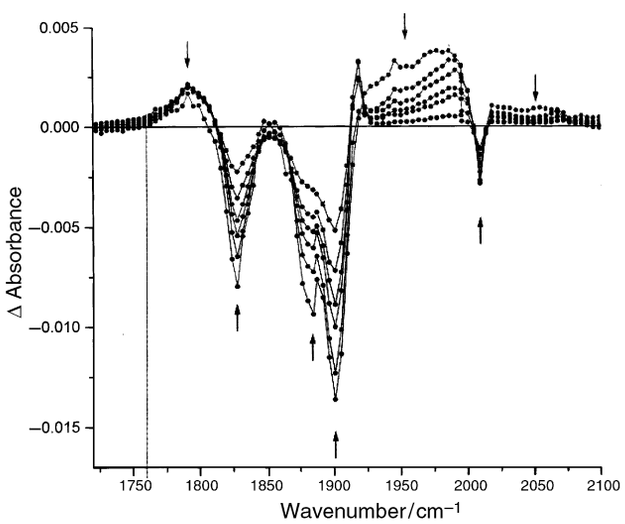

Fig. 8 Time-resolved infrared absorption spectra of $[Cr(CO)_4(bpy)]$ in CH_2Cl_2 solution, recorded at various time-delays after 400 nm, ≈200 fs (FWHM) excitation. The 1720–2100 cm^{-1} region shown here was covered by overlapping three separate 'spectral windows', each approximately 200 cm^{-1} wide. Spectra were measured at 1, 10, 30, 50, 100 and 1000 ps after excitation. Arrows (↑ and ↓) denote portions of the spectrum which are increasing or decreasing in intensity.

The results shown in Fig. 8 clearly manifest the power of ps TR-IR experiments in understanding organometallic photochemical mechanisms. The negative bands at 1827, 1884, 1901 and 2009 cm^{-1} are a mirror image of the ground-state $[Cr(CO)_4(bpy)]$ IR spectrum and result from ground state depletion on excitation. The broad, rapidly decaying IR absorption in the region 1925–2075 cm^{-1} is consistent with formation of ^{3}MLCT trapping states, since the ν(CO) peaks are shifted

upwards from their ground state values.[67,68] This reflects the decrease in electron density on the Cr atom and, hence, of Cr⟶CO π back-donation upon Cr⟶bpy MLCT excitation. The composite character and broadness of this transient absorption indicates that one or more ^{3}MLCT states are present and may also suggest that such species are formed vibrationally hot. Decay kinetics of the IR absorption due to these ^{3}MLCT states parallels the partial recovery of the ground state IR absorption, with biexponential kinetics which correspond to that found in TR-visible absorption spectroscopy. Thus, the ps TR-IR spectra have confirmed our initial assumption that the ^{3}MLCT states are trapping states which are not involved in CO dissociation, instead decaying directly into the ground state. IR bands due to the photoproduct *fac*-[Cr(L)(CO)$_3$(bpy)] were found at 1791(br) and 1919 cm^{-1}, the latter band overlapping with the negative bleached ground-state absorption, which makes it observable only at longer time delays, after the bleach has partially decayed. Importantly, the 1791 cm^{-1} photoproduct band is present from the earliest time-delays of 1 ps with an almost time-independent intensity. This observation confirms that CO dissociation and population of the trapping ^{3}MLCT states are indeed parallel processes which occur on an ultrafast time scale from the optically prepared Franck–Condon excited state. Notably, the shape, number and positions of the photoproduct IR bands, measured on a ps time scale, are the same as those determined at 10 ns. As is explained in our previous nanosecond study,[65] the photoproduct IR spectrum belongs to *fac*-[Cr(L)(CO)$_3$(bpy)] (L = CH_2Cl_2). The ps TR-IR spectra thus show that the photoproduct has the facial geometry already at 1 ps. Since it is very unlikely that *mer*⟶*fac* isomerisation following photodissociation of an equatorial CO ligand would occur with a sub-picosecond rate, we can reasonably conclude that the *fac*-isomer is the primary photoproduct. This conclusion implies that the photofragmentation of [Cr(CO)$_4$(bpy)] involves a very selective splitting of one axial Cr–CO bond.

This case study of CO photodissociation from [Cr(CO)$_4$-(bpy)] shows how precise kinetic data can be obtained from ultrafast time-resolved visible absorption spectroscopy and a plausible photochemical mechanism deduced. However, confirmation of the mechanism requires the direct observation of the temporal behaviour of the individual species involved and their structural characterisation. Time-resolved IR absorption spectroscopy is very well suited to this purpose. In the particular case of the photochemistry of [Cr(CO)$_4$(bpy)], TR-IR has allowed us to: (i) characterize the trapping states as MLCT; (ii) prove that the decay of the trapping states leads to the ground state; (iii) prove that the CO-loss photoproduct is formed within the instrument time resolution (<400 fs) and (iv) identify the photoproduct at 1 ps as *fac*-[Cr(L)(CO)$_3$(bpy)], indicating the high selectivity of the ultrafast bond-splitting reaction.

Dissociative isomerisation of [Mn(Br)(CO)$_3$(iPr-DAB)]

Irradiation of [Mn(Br)(CO)$_3$(iPr-DAB)] solutions in various solvents with visible light leads to the dissociation of a CO ligand and movement of the Br ligand from the axial to an equatorial position.[69,70] In non-coordinating solvents such as CH_2Cl_2, CO re-binds to the Mn atom and the reaction results in a *fac*⟶*mer* isomerization. In contrast, in strongly coordinating solvents (Solv) such as pyridine, the CO is replaced by the solvent, effectively halting the reaction with the formation of [Mn(Br)(Solv)(CO)$_2$(iPr-DAB)].[69] This is shown in Scheme 2, however, the detailed mechanism of this photochemical isomerisation is not known. The reaction is triggered by optical excitation of [Mn(Br)(CO)$_3$(iPr-DAB)] into its MLCT/XLCT mixed-character excited state, whereby the electron density is transferred from a Mn(d_π)–Br(p_π) orbital to the π* orbital of the iPr-DAB ligand.[71,72] (The acronym MLCT stands for metal

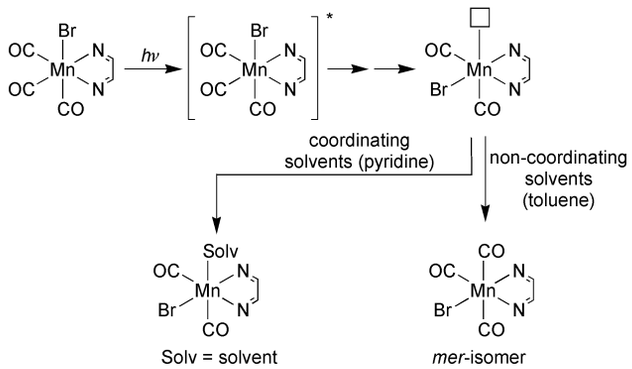

Scheme 2 Dissociative isomerisation of *fac*-[Mn(Br)(CO)$_3$(iPr-DAB)]. □ represents the vacant coordination position.

to ligand charge transfer while XLCT represents halide(X) to ligand charge transfer.) DFT calculations of the excited state potential energy surfaces along various coordinates have indicated large energy barriers for dissociation of either the axial or equatorial CO ligand.[72] These calculations have suggested that dissociation of the equatorial CO ligand, concerted with the movement of the Br ligand from the axial to the equatorial position, is energetically the most favourable pathway, albeit still involving a large energy barrier. To explain the observed reactivity, it was proposed that the reaction involves resonance coupling between the MLCT/XLCT excited state and the dissociative ground-state continuum.[72] Such a process would be expected to occur with a probability less than that of direct dissociation of a CO ligand from a repulsive excited state, for example, as is known for M(CO)$_6$ (M = Cr, Mo, W)[33] or for the [Cr(CO)$_4$(bpy)] complex discussed above. Hence, the primary photochemical reaction step of the dissociative isomerisation of [Mn(Br)(CO)$_3$(iPr-DAB)] is expected to occur on a time scale considerably longer than the 20–400 fs range of the direct CO dissociation.

Shown in Fig. 9 are the time-resolved visible absorption

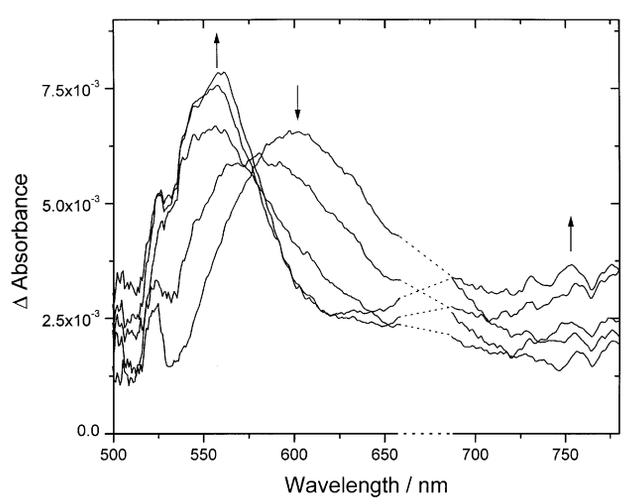

Fig. 9 Time-resolved visible absorption spectra of *fac*-[Mn(Br)(CO)$_3$(^{i}Pr-DAB)] in pyridine solution, recorded at various time-delays after 500 nm, ≈200 fs (FWHM) excitation in the region 500–780 nm. From top to bottom (at 605 nm): spectra measured at 2, 6, 16, 50 and 200 ps after excitation. Five-point adjacent averaging was applied to smooth the data. The area represented by dotted lines is obscured by an experimental artefact.

spectra of [Mn(Br)(CO)$_3$(iPr-DAB)] measured from pyridine solution. A species characterised by an absorption band at 605 nm is formed within the instrument time resolution (*ca.* 400 fs). This band decays with an 11 ps lifetime while another band with an apparent maximum at 560 nm, grows in with identical kinetics and persists on longer time scales.

This behaviour demonstrates that the initially formed species undergoes a conversion into the photoproduct with a time constant of 11 ps. In addition, the 560 nm photoproduct band shows a minor 22 ps kinetic component. A weak absorption in the red spectral region (>700 nm) grows in with the same 22 ps time constant. This experiment provides a clear kinetic picture, but it allows at least two possible mechanistic interpretations:

(a) Guided by the DFT calculations,[72] the 605 nm band is attributed to the MLCT/XLCT excited state and the 11 ps process to the concerted CO dissociation and Br movement. The small changes, occurring with the 22 ps time constant, can be explained by structural relaxation, which involves coordination of a pyridine molecule at the axial position, and by structural adjustment of the Br ligand in the equatorial position.

(b) Alternatively, it can be assumed that either the axial or equatorial CO ligand leaves on the femtosecond time scale, as it does in other carbonyl complexes. In this case, CO dissociation is completed within the instrument time resolution and the species absorbing at 605 nm can be identified as the primary photoproduct, that is the solvated CO-loss species [Mn(Br)-$(CO)_2$(iPr-DAB)]. The 11 ps process, then, corresponds to the axial⟶equatorial Br movement, which is now subsequent to the CO dissociation. The final 22 ps process is again interpreted as a full pyridine coordination and accompanying structural relaxation.

This mechanistic ambiguity stems from the fact that it is often difficult to distinguish between a primary photoproduct and an excited state using TR-visible absorption spectra only. In the particular case of [Mn(Br)$(CO)_3$(iPr-DAB)], we may expect that the main visible absorption band will shift from 480 nm to longer wavelengths, due to increased electron density on the Mn atom upon the loss of a π-accepting CO ligand. At the same time, however, the MLCT/XLCT state can also be expected to absorb at around 600 nm due to the presence of a iPr-DAB$^{\bullet-}$ chromophore.[73] Picosecond TR-infrared spectroscopy is the technique of choice to probe the difference between an excited state of [Mn(Br)$(CO)_3$(iPr-DAB)] and the [Mn(Br)-$(CO)_2$(iPr-DAB)] primary photoproduct. The IR spectrum of the MLCT/XLCT excited state is expected to show the same ν(CO) IR pattern as the ground state, but shifted to higher wavenumbers by 20–40 cm^{-1}. (This shift is estimated from the nanosecond TR-IR spectrum of [Ru(I)(Me)(CO)(iPr-DAB)] which has a long-lived, MLCT/XLCT excited state.)[74] On the other hand, the [Mn(Br)$(CO)_2$(iPr-DAB)] primary photoproduct should exhibit two IR bands, shifted to lower frequencies from those of [Mn(Br)$(CO)_3$(iPr-DAB)]. This is due to an increase in Mn⟶CO π back-donation into the remaining two CO ligands, caused by the loss of one of the original three π-accepting CO ligands.

Shown in Fig. 10 is the TR-IR spectrum of [Mn(Br)$(CO)_3$-(iPr-DAB)] in pyridine solution measured at 2 ps after excitation. The absence of any new IR bands at frequencies higher than that of the ground state precludes the possibility that the initially formed species is the XLCT/MLCT excited state. A new IR absorption band arises at 1970 cm^{-1}, together with a very weak, broad absorption centred at *ca.* 1825 cm^{-1}. This experiment indicates that the primary photochemical step in the dissociative isomerization of [Mn(Br)$(CO)_3$(iPr-DAB)] is an ultrafast (<400 fs) CO dissociation, similar to that occurring in other metal carbonyls and described above for [Cr$(CO)_4$(bpy)]. The isomerisation step occurs *via* Br movement, subsequent to CO dissociation. The experimental data summarised above are consistent with the following mechanism:

$$fac\text{-}[Mn(Br)(CO)_3(iPr\text{-}DAB)] \xrightarrow{h\nu} \quad (4)$$

$$*[Mn(Br)(CO)_3(iPr\text{-}DAB)] \xrightarrow{<400\ fs} ax\text{-}[Mn(Br)(CO)_2(iPr\text{-}DAB)]$$

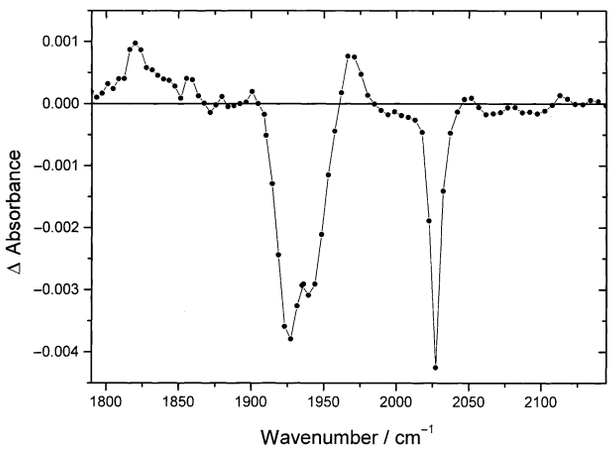

Fig. 10 Time-resolved infrared absorption spectrum of *fac*-[Mn(Br)-$(CO)_3$(^{i}Pr-DAB)] in pyridine-d_5 solution, recorded 2 ps after 500 nm, ≈200 fs (FWHM) excitation. The 1790–2145 cm^{-1} region shown here was covered by overlapping three separate 'spectral windows', each recording approximately 200 cm^{-1} of the total coverage.

$$ax\text{-}[Mn(Br)(CO)_2(iPr\text{-}DAB)] \xrightarrow{11\ ps} eq\text{-}[Mn(Br)(CO)_2(iPr\text{-}DAB)] \quad (5)$$

$$eq\text{-}[Mn(Br)(CO)_2(iPr\text{-}DAB)] \xrightarrow{+L,\ 22\ ps} eq\text{-}[Mn(Br)(L)(CO)_2(iPr\text{-}DAB)] \quad (6)$$

where the *ax* and *eq* prefixes specify the position of the Br ligand with respect to the Mn(DAB) plane (axial and equatorial, respectively). In reality, the dicarbonyl intermediates are weakly solvated and the last step involves a change of pyridine bonding, from solvation to coordination. The TR-IR experiments are complicated by broadening and overlap of transient bands which prevent us, at the moment, from determining the position (*ax* or *eq*) of the initially dissociated CO ligand. Besides, further research is under way to examine the alternative reaction mechanisms, such as those involving LF excited states. It will also be important to decide whether the *ax*⟶*eq* movement of the Br ligand is a part of vibrational cooling of a "hot" primary photoproduct.[75]

Interligand electron transfer in [Re(MQ$^+$)$(CO)_3$(dmb)]$^{2+}$: time-resolved visible and IR absorption and resonance Raman spectroscopy

Irradiation of [Re(MQ$^+$)$(CO)_3$(dmb)]$^{2+}$ (MQ$^+$ = *N*-methyl-4,4′-bipyridinium, dmb = 4,4′-dimethyl-2,2′-bipyridine) in the near UV region (330–400 nm) simultaneously populates Re⟶dmb and Re⟶MQ$^+$ metal-to-ligand charge transfer excited states, abbreviated hereinafter as MLCT(dmb) and MLCT(MQ$^+$), respectively. The MLCT(dmb) state can be viewed as [Re^{II}-(MQ$^+$)$(CO)_3$(dmb$^{\bullet-}$)]$^{2+}$. Its population is followed by an interligand electron transfer (7) from dmb$^{\bullet-}$ to MQ$^+$, which produces a relaxed MLCT(MQ$^+$) excited state that can be formulated as [Re^{II}(MQ$^{\bullet}$)$(CO)_3$(dmb)]$^{2+}$, see Scheme 3.[59,76–79]

$$[Re^{II}(MQ^+)(CO)_3(dmb^{\bullet-})]^{2+} \longrightarrow [Re^{II}(MQ^{\bullet})(CO)_3(dmb)]^{2+} \quad (7)$$

The identity of the [Re^{II}(MQ$^+$)$(CO)_3$(dmb$^{\bullet-}$)]$^{2+}$ electron-transfer product has been established earlier by resonance Raman spectroscopy, using intense single-colour nanosecond laser pulses, and by nanosecond TR-visible absorption.[78,79] Both these techniques have shown spectroscopic signatures typical of the quinoidal MQ$^{\bullet}$ ligand. In order to understand the dynamics of this reaction, we have measured fs–ps TR-visible absorption spectra in acetonitrile and ethylene glycol. The

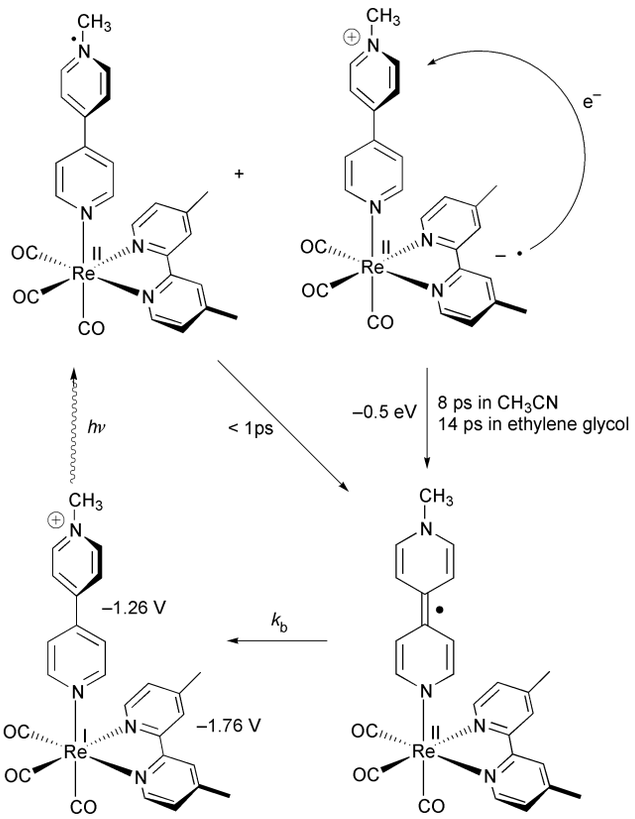

Scheme 3 Excited-state interligand electron transfer in *fac*-[Re(MQ)-$(CO)_3$(dmb)]$^{2+}$.

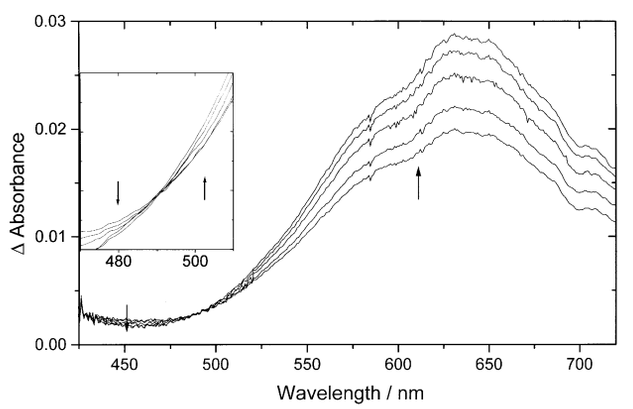

Fig. 11 Time-resolved visible absorption spectra of *fac*-[Re(MQ)-$(CO)_3$(dmb)]$^{2+}$ in acetonitrile solution, recorded at various time-delays after 500 nm, ≈200 fs (FWHM) excitation. Each spectrum was measured with a white light continuum probe beam. Spectra were measured at 2, 4, 8, 16 and 30 ps after excitation. The inset shows an expansion of the region 470–510 nm with an isosbestic point at *ca.* 490 nm.

results of this study are presented in Fig. 11. The spectra show a weak absorption in the 420–470 nm region and a very strong band centred at 640 nm. The former absorption is characteristic of the dmb$^{\bullet-}$ chromophore[59,80] and was attributed to the MLCT(dmb) excited state [$Re^{II}(MQ^+)(CO)_3(dmb^{\bullet-})$]$^{2+}$. The 640 nm band belongs to the MQ$^{\bullet}$ chromophore of the MLCT-(MQ^+) state, that is the [$Re^{II}(MQ^{\bullet})(CO)_3$(dmb)]$^{2+}$ electron-transfer product.[78,79] Both these absorption bands are present already in the spectra taken at the earliest time delays, in accordance with the proposed simultaneous population of the MLCT(dmb) and MLCT(MQ^+) excited states on 400 nm excitation, Scheme 3. The following spectral evolution shows that the MLCT(dmb) absorption decays concomitantly with the rise of the MLCT(MQ^+) band at 640 nm. The presence of an isosbestic point and the observation of identical kinetics for the absorbance decay in the 420–470 nm region and the rise between 600 and 640 nm show that the reaction (7) occurs as a clean, direct conversion of the MLCT(dmb) state into the MLCT(MQ^+) state. The time constant of this interligand electron transfer was determined[59] as 8.3 ± 0.4 ps in CH_3CN and 14.0 ± 1.6 ps in ethylene glycol. The two-fold decrease of the reaction rate on going from CH_3CN to ethylene glycol was interpreted as a change of the electron transfer mechanism from non-adiabatic to partly adiabatic.[59] This could be caused by the change of the solvent relaxation time which is much faster than the ET reaction in CH_3CN but slower or comparable in ethylene glycol. However, the actual situation might be more complicated since the electron transfer could proceed *via* a through-solvent tunneling mechanism.[81] In this case, the electronic coupling between the dmb$^{\bullet-}$ donor and MQ^+ acceptor ligands would be solvent-dependent. Moreover, the activation of specific high-frequency vibrations can contribute to the adiabatic reaction rate, the interring ν(CC) vibration being the main suspect.

Although the fs–ps TR-visible absorption spectra have afforded a straightforward mechanistic picture and accurate kinetic data, some important questions concerning the interligand electron transfer remain unanswered: (i) Are some of the high-frequency vibrations activated during the interligand electron transfer and does this activation persist on a longer time scale? (ii) Is the electron transfer product formed vibrationally relaxed or is it initially hot (excited)? (iii) Are the vibrational relaxation dynamics solvent-dependent? (iv) Is the $Re(CO)_3$ moiety affected by the interligand electron transfer? To answer these questions, it is necessary to resort to time-resolved vibrational spectroscopic techniques, namely ps time-resolved resonance Raman (TR^3) and IR absorption spectroscopies.

Shown in Fig. 12 are the TR^3 spectra of [Re(MQ^+)-

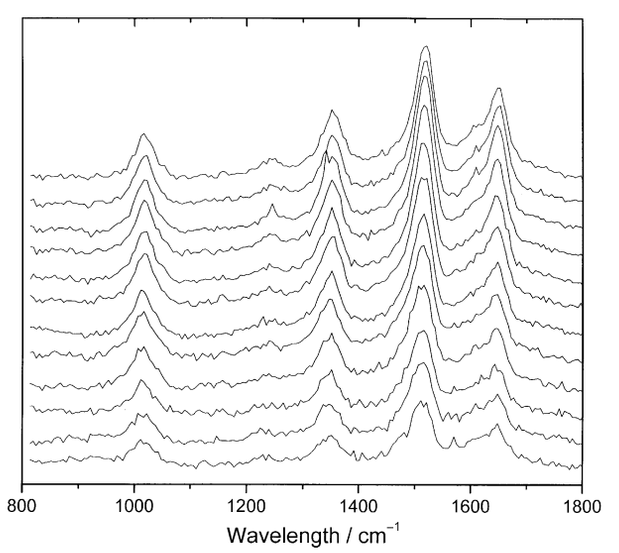

Fig. 12 Time-resolved resonance Raman spectra (TR^3) of *fac*-[Re(MQ^+)$(CO)_3$(dmb)]$^{2+}$ in acetonitrile solution after 400 nm, 1 ps (FWHM) excitation. Spectra were recorded using a 600 nm, 1 ps pulse and a grating spacing of 1200 groves mm^{-1}. A 4 ps Kerr gate was employed to reject sample fluorescence from the collected light. It was opened at the time of the measurement for *ca.* 3 ps. From bottom to top: spectra recorded at 1, 2, 3, 5, 7, 10, 15, 20, 30, 50, 100 and 500 ps.

$(CO)_3$(dmb)]$^{2+}$, in CH_3CN solution, measured between 1 and 500 ps after laser pulse excitation at 400 nm. The spectra were measured with Raman probe wavelength of 600 nm, that is in resonance with the MQ$^{\bullet}$ absorption band. Only Raman bands due to vibrations of the MQ$^{\bullet}$ ligand are visible: $\nu(CC)_{ir}/\nu(CC)$ 1647 cm^{-1}; $\nu(CN)/\gamma(CCH)$ 1516 cm^{-1}; $\gamma(CCH)/\nu(CC)_{ir}$ 1352 cm^{-1} and $\gamma(CCN)/\nu(CN)$ 1018 cm^{-1}. (Peak positions extrapolated to long time delays. $(CC)_{ir}$ denotes the inter-ring

C–C bond. Assignment is based on the results of previous studies.)[79,82] All of the $MQ^{\bullet}$ Raman peaks are already present in the spectra measured at 1 ps with low intensities. Their integrated intensities then grow with a time constant approximately equal to that of the electron transfer reaction (7). Over time, the Raman peak positions show a dynamic shift by 4–7 cm^{-1} to higher wavenumbers. This shift depends exponentially on time for all of the bands studied and the corresponding time-constant depends on the particular peak and the solvent. In CH_3CN, time constants of *ca.* 24, 16 and 15 ps were determined for the peaks at 1516, 1352 and 1018 cm^{-1}, respectively. (The highest peak also shifts upwards, but its analysis is complicated since it is composed of two peaks with variable positions and widths.) The widths of the Raman peaks decrease, with time constants slightly lower than those found for the peak shifts: 17, 11 and 13 ps, respectively. Surprisingly, the peak-shifting and peak-narrowing time constants are lower in ethylene glycol, where they lie in the range 15–11 ps and at *ca.* 7 ps, respectively, indicating faster relaxation rates. The absolute values of the dynamic peak shifts, however, are small in both solvents. Hence, it is obvious that all of the observed Raman peaks occur very close to their final positions even at the earliest time delays measured, that is at 1–2 ps. This is especially obvious for the 1352 cm^{-1} peak that is up-shifted with respect to its ground-state position by *ca.* 55 cm^{-1} at 1 ps and 61 cm^{-1} at 500 ps. There is no relationship between the magnitude or rate of the dynamic peak shift of a particular Raman peak and the difference between the corresponding peak wavenumbers of the $[Re(MQ^+)(CO)_3(dmb)]^{2+}$ ground state and the $[Re^{II}(MQ^{\bullet})(CO)_3(dmb)]^{2+}$ electron-transfer product. Moreover, no anti-Stokes peaks were observed in the ps TR^3 spectrum. Hence, it can be concluded that promoted high-frequency modes relax either more quickly than, or alongside, the $dmb^{\bullet-} \longrightarrow MQ^+$ interligand electron transfer. There is no evidence for any specific activation of high-frequency vibrations in the ET product $[Re^{II}(MQ^{\bullet})(CO)_3(dmb)]^{2+}$. At the same time, the small upward dynamic shifts and broadening of the $MQ^{\bullet}$ Raman peaks show that the extra energy (*ca.* 0.5 eV) discharged in the reaction (7) is rapidly redistributed into many low-frequency vibrations, leaving the $[Re^{II}(MQ^{\bullet})(CO)_3(dmb)]^{2+}$ electron-transfer product initially vibrationally hot. The final relaxation then follows on a time scale of a few tens of picoseconds.

The final piece of mechanistic information concerning the interligand electron transfer reaction (7) comes from picosecond time-resolved IR absorption spectroscopy, Fig. 13. The spectra of $[Re(MQ^+)(CO)_3(dmb)]^{2+}$ measured at early times after excitation show very weak bands at 1960 and 2010 cm^{-1} and a stronger band at 2060 cm^{-1}. This spectral pattern is typical of the MLCT(dmb) excited state $[Re^{II}(MQ^+)(CO)_3(dmb^{\bullet-})]^{2+}$, as was determined by comparison with the independently measured TR-IR spectrum of the analogous $[Re(Et\text{-}py)(CO)_3(dmb)]^+$ complex, in which no electron transfer occurs (Et-py = 4-ethylpyridine). The upward shift of the ν(CO) wavenumbers from their ground state values is caused by the depopulation of $Re(d_\pi)$ orbitals upon Re⟶dmb MLCT excitation which, in turn, diminishes the amount of Re⟶CO π back-donation.[67,68,83] Additionally, a weak band at 2100 cm^{-1} is present in the spectrum already at 1 ps. Subsequently, its intensity increases with a time constant approximately equal to that of the electron transfer reaction (7), accompanied by an emergence of a weak, broad band at 1997 cm^{-1}. Intensities of the $[Re^{II}(MQ^+)(CO)_3(dmb^{\bullet-})]^{2+}$ bands decrease concomitantly. The new spectral pattern (1997(w, broad), 2100(s) cm^{-1}) corresponds to the electron-transfer product $[Re^{II}(MQ^{\bullet})(CO)_3(dmb)]^{2+}$. The large difference between the IR spectral patterns of $[Re^{II}(MQ^+)(CO)_3(dmb^{\bullet-})]^{2+}$ and $[Re^{II}(MQ^{\bullet})(CO)_3(dmb)]^{2+}$ is rather surprising. It shows that the $[Re^{II}(MQ^+)(CO)_3(dmb^{\bullet-})]^{2+} \longrightarrow [Re^{II}(MQ^{\bullet})(CO)_3(dmb)]^{2+}$ electron transfer (7) is accompanied by significant structural changes of the $Re(CO)_3$ moiety. The upward shift of the highest ν(CO) band indicates that Re⟶CO π back-donation is weaker in $[Re^{II}(MQ^{\bullet})(CO)_3(dmb)]^{2+}$ than $[Re^{II}(MQ^+)(CO)_3(dmb^{\bullet-})]^{2+}$. This can be due to greater localization of the excited electron at the $MQ^{\bullet}$ ligand, as compared with $dmb^{\bullet-}$.

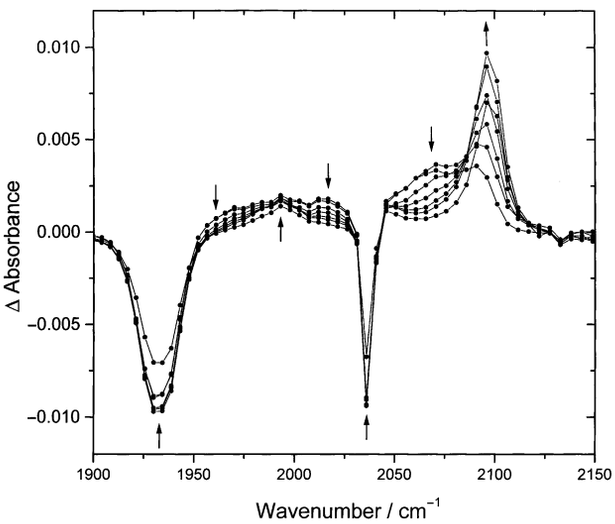

Fig. 13 Time-resolved infrared absorption spectrum of *fac*-$[Re(MQ^+)(CO)_3(dmb)]^{2+}$ in acetonitrile solution, recorded at various time-delays following 500 nm, ≈200 fs (FWHM) excitation. Spectra recorded at 1, 2, 4, 8, 16, 36 and 1000 ps. Arrows (↑ and ↓) show portions of the spectrum which are increasing or decreasing in intensity.

To summarize, picosecond TR-visible absorption spectra of $[Re(MQ^+)(CO)_3(dmb^{\bullet-})]^{2+}$ have allowed us to determine accurately the kinetics of the interligand electron transfer reaction (7) and to identify both excited states involved. The latter was made possible by the fact that the $dmb^{\bullet-}$ and $MQ^{\bullet}$ chromophores, present in the initial and final states, respectively, have characteristic absorption bands in the visible spectral region. TR-vibrational spectroscopy has confirmed this mechanism and provided additional information on the details of the electron transfer reaction. More specifically, ps TR-IR and TR^3 experiments have shown that the electron transfer is accompanied by very fast energy dissipation from ν(CO) and $MQ^{\bullet}$ high-frequency vibrations. The small time-dependent shifts of Raman peaks observed by TR^3 show that at least part of this energy redistribution is intramolecular, into low-frequency skeletal modes. Moreover, TR-IR spectra indicate that the interligand electron transfer is accompanied by structural changes in the $Re(CO)_3$ moiety.

Conclusions

Early excited-state dynamics often determine the photochemistry of organometallic compounds and transition metal complexes. The structure and dynamical behaviour, namely relaxation, electron transfer and fragmentation, of excited states and photointermediates can now be studied in a real time using femtosecond–picosecond time-resolved spectroscopic techniques. Combined studies of time-resolved absorption in the visible and infrared spectral regions with time-resolved resonance Raman and emission proved to be especially useful in revealing the ultrafast steps of organometallic photochemical reactions and characterizing the transient species involved.

Acknowledgements

This work was supported by EPSRC. A. V. and I. R. F. also thank the CLRC Rutherford Appleton Laboratory for the experimental time provided.

References

1 A. H. Zewail, *Angew. Chem., Int. Ed.*, 2000, **39**, 2586.
2 A. H. Zewail, *J. Phys. Chem. A*, 2000, **104**, 5660.
3 A. Vlček, Jr., *Coord. Chem. Rev.*, 2000, **200–202**, 933.
4 Y. Tachibana, J. E. Moser, M. Grätzel, D. R. Klug and J. R. Durrant, *J. Phys. Chem.*, 1996, **100**, 20056.
5 B. Burfeindt, T. Hannappel, W. Storck and F. Willig, *J. Phys. Chem.*, 1996, **100**, 16463.
6 M. Hilgendorff and V. Sundström, *J. Phys. Chem. B*, 1998, **102**, 10505.
7 R. J. Ellingson, J. B. Asbury, S. Ferrere, H. N. Ghosh, J. R. Sprague, T. Lian and A. J. Nozik, *J. Phys. Chem. B*, 1998, **102**, 6455.
8 H. N. Ghosh, J. B. Asbury, Y. Weng and T. Lian, *J. Phys. Chem. B*, 1998, **102**, 10208.
9 J. B. Asbury, R. J. Ellingson, H. N. Ghosh, S. Ferrere, A. J. Nozik and T. Lian, *J. Phys. Chem. B*, 1999, **103**, 3110.
10 Y. Tachibana, S. A. Haque, I. P. Mercer, J. R. Durrant and D. R. Klug, *J. Phys. Chem. B*, 2000, **104**, 1198.
11 J. B. Asbury, E. Hao, Y. Wang, H. N. Ghosh and T. Lian, *J. Phys. Chem. B*, 2001, **105**, 4545.
12 S. Ferrere and B. A. Gregg, *J. Am. Chem. Soc.*, 1998, **120**, 843.
13 S. Engleitner, M. Seel and W. Zinth, *J. Phys. Chem. A*, 1999, **103**, 3013.
14 P. J. Reid, C. Silva, P. F. Barbara, L. Karki and J. T. Hupp, *J. Phys. Chem.*, 1995, **99**, 2609.
15 D. LeGourriérec, M. Andersson, J. Davidsson, E. Mukhtar, L. Sun and L. Hammarström, *J. Phys. Chem. A*, 1999, **103**, 557.
16 A. S. Lukas, S. E. Miller and M. R. Wasielewski, *J. Phys. Chem. B*, 2000, **104**, 931.
17 M. A. Ratner and J. Jortner, in *Molecular Electronics: Some Directions*, ed. J. Jortner and M. Ratner, Oxford, 1997.
18 N. H. Damrauer, G. Cerullo, A. Yeh, T. R. Boussie, C. V. Shank and J. K. McCusker, *Science*, 1997, **275**, 54.
19 A. T. Yeh, C. V. Shank and J. K. McCusker, *Science*, 2000, **289**, 935.
20 N. H. Damrauer and J. K. McCusker, *J. Phys. Chem. A*, 1999, **103**, 8440.
21 J. E. Monat and J. K. McCusker, *J. Am. Chem. Soc.*, 2000, **122**, 4092.
22 M. R. Waterland and D. F. Kelley, *J. Phys. Chem. A*, 2001, **105**, 4019.
23 E. J. C. Olson, D. Hu, A. Hormann, A. M. Jonkman, M. R. Arkin, E. D. A. Stemp, J. K. Barton and P. F. Barbara, *J. Am. Chem. Soc.*, 1997, **119**, 11458.
24 B. Önfelt, P. Lincoln, B. Nordén, J. S. Baskin and A. H. Zewail, *Proc. Natl. Acad. Sci. USA*, 2000, **97**, 5708.
25 J. B. Asbury, K. Hang, J. S. Yeston, J. G. Cordaro, R. G. Bergman and T. Lian, *J. Am. Chem. Soc.*, 2000, **122**, 12870.
26 S. E. Bromberg, H. Yang, M. C. Asplund, T. Lian, B. K. McNamara, K. T. Kotz, J. S. Yeston, M. Wilkens, H. Frei, R. G. Bergman and C. B. Harris, *Science*, 1997, **278**, 260.
27 R. Osman, R. N. Perutz, A. D. Rooney and A. J. Langley, *J. Phys. Chem.*, 1994, **98**, 3562.
28 M. Colombo, M. W. George, J. N. Moore, D. I. Pattison, R. N. Perutz, I. G. Virrels and T.-Q. Ye, *J. Chem. Soc., Dalton Trans.*, 1997, 2857.
29 P. T. Snee, C. K. Payne, K. T. Kotz, H. Yang and C. B. Harris, *J. Am. Chem. Soc.*, 2001, **123**, 2255.
30 B. Klingert, M. Riediker and A. Roloff, *Commun. Inorg. Chem.*, 1988, **7**, 109.
31 S. K. Weit, C. Kutal and R. D. Allen, *Chem. Mater.*, 1992, **4**, 453.
32 V. Jakúbek and A. J. Lees, *Inorg. Chem.*, 2000, **39**, 5779.
33 T. Lian, S. E. Bromberg, M. C. Asplund, H. Yang and C. B. Harris, *J. Phys. Chem.*, 1996, **100**, 11994.
34 S. E. Bromberg, T. Lian, R. G. Bergman and C. B. Harris, *J. Am. Chem. Soc.*, 1996, **118**, 2069.
35 I. R. Farrell, P. Matousek and A. Vlček, Jr., *J. Am. Chem. Soc.*, 1999, **121**, 5296.
36 I. R. Farrell and A. Vlček, Jr., *Coord. Chem. Rev.*, 2000, **208**, 87.
37 H. Yang, K. T. Kotz, M. C. Asplund, M. J. Wilkens and C. B. Harris, *Acc. Chem. Res.*, 1999, **32**, 551.
38 D. E. Spence, P. N. Kean and W. W. Sibbett, *Opt. Lett.*, 1991, **16**, 42.
39 W. Sibbett, D. T. Reid and M. Ebrahimzadeh, *Phil. Trans. R. Soc. Lond. A*, 1998, **356**, 283.
40 I. R. Farrell, P. Matousek, C. J. Kleverlaan and A. Vlček, Jr., *Chem. Eur. J.*, 2000, **6**, 1386.
41 J. P. Cushing, C. Butoi and D. F. Kelley, *J. Phys. Chem. A*, 1997, **101**, 7222.
42 P. Matousek, R. E. Hester, J. N. Moore, A. W. Parker, D. Phillips, W. T. Toner, M. Towrie, I. C. E. Turcu and S. Umapathy, *Meas. Sci. Technol.*, 1993, **4**, 1090.
43 P. Matousek, A. W. Parker, P. F. Taday, W. T. Toner and M. Towrie, *Opt. Commun.*, 1996, **127**, 307.
44 M. Towrie, A. W. Parker, W. Shaikh and P. Matousek, *Meas. Sci. Technol.*, 1998, **9**, 816.
45 A. Penzkofer, A. Beidoun and H. J. Lehmeier, *Opt. Quantum Electron.*, 1993, **25**, 317.
46 Q. R. Xing, K. M. Yoo and R. R. Alfano, *Appl. Opt.*, 1993, **32**, 2087.
47 W. L. Smith, P. Liu and N. Bloembergen, *Phys. Rev. A*, 1977, **15**, 2396.
48 M. Towrie, D. C. Grills, P. Matousek, A. W. Parker and M. W. George, *Appl. Spectrosc.*, 2002, in press.
49 F. Seifert, V. Petrov and M. Woerner, *Opt. Lett.*, 1994, **19**, 2009.
50 P. Hamm, C. Lauterwasser and W. Zinth, *Opt. Lett.*, 1993, **18**, 1943.
51 V. Petrov, Y. Tanaka and T. Suzuki, *IEEE J. Quantum Electron.*, 1997, **33**, 1749.
52 M. K. Reed and M. K. S. Shepard, *IEEE J. Quantum Electron.*, 1996, **32**, 1273.
53 U. Emmerichs, H. J. Bakker and H. Kurz, *Opt. Commun.*, 1994, **111**, 497.
54 M. Cavallari, G. M. Gale, F. Hache, L. I. Pavlov and E. Rousseau, *Opt. Commun.*, 1995, **114**, 329.
55 K. L. Vodopyanov and V. Chazapis, *Opt. Commun.*, 1997, **135**, 98.
56 P. Matousek, M. Towrie, A. Stanley and A. W. Parker, *Appl. Spectrosc.*, 1999, **53**, 1485.
57 P. Matousek, M. Towrie, C. Ma, W. M. Kwok, D. Phillips, W. T. Toner and A. W. Parker, *J. Raman Spectrosc.*, 2001, **32**, 983.
58 I. R. Farrell, P. Matousek and A. Vlček, Jr., *Inorg. Chem.*, to be submitted.
59 D. J. Liard and A. Vlček, Jr., *Inorg. Chem.*, 2000, **39**, 485.
60 R. W. Balk, T. Snoeck, D. J. Stufkens and A. Oskam, *Inorg. Chem.*, 1980, **19**, 3015.
61 S. Wieland, K. B. Reddy and R. van Eldik, *Organometallics*, 1990, **9**, 1802.
62 W. F. Fu and R. van Eldik, *Inorg. Chim. Acta*, 1996, **251**, 341.
63 W.-F. Fu and R. van Eldik, *Inorg. Chem.*, 1998, **37**, 1044.
64 J. Víchová, F. Hartl and A. Vlček, Jr., *J. Am. Chem. Soc.*, 1992, **114**, 10903.
65 I. G. Virrels, M. W. George, J. J. Turner, J. Peters and A. Vlček, Jr., *Organometallics*, 1996, **15**, 4089.
66 B. C. Noble and R. D. Peacock, *Spectrochim. Acta, Part A*, 1990, **46**, 407.
67 P. Glyn, M. W. George, P. M. Hodges and J. J. Turner, *J. Chem. Soc., Chem. Commun.*, 1989, 1655.
68 M. W. George, F. P. A. Johnson, J. R. Westwell, P. M. Hodges and J. J. Turner, *J. Chem. Soc., Dalton Trans.*, 1993, 2977.
69 G. J. Stor, S. L. Morrison, D. J. Stufkens and A. Oskam, *Organometallics*, 1994, **13**, 2641.
70 C. J. Kleverlaan, F. Hartl and D. J. Stufkens, *J. Photochem. Photobiol. A: Chem.*, 1997, **103**, 231.
71 G. J. Stor, D. J. Stufkens, P. Vernooijs, E. J. Baerends, J. Fraanje and K. Goubitz, *Inorg. Chem.*, 1995, **34**, 1588.
72 A. Rosa, G. Ricciardi, E. J. Baerends and D. J. Stufkens, *J. Phys. Chem.*, 1996, **100**, 15346.
73 B. D. Rossenaar, C. J. Kleverlaan, M. C. E. van de Ven, D. J. Stufkens and A. Vlček, Jr., *Chem. Eur. J.*, 1996, **2**, 228.
74 M. P. Aarnts, D. J. Stufkens, M. P. Wilms, E. J. Baerends, A. Vlček, Jr., I. P. Clark, M. W. George and J. J. Turner, *Chem. Eur. J.*, 1996, **2**, 1556.
75 M. Poliakoff, *Inorg. Chem.*, 1976, **15**, 2892.
76 T. D. Westmoreland, H. Le Bozec, R. W. Murray and T. J. Meyer, *J. Am. Chem. Soc.*, 1983, **105**, 5952.
77 P. Chen, M. Curry and T. J. Meyer, *Inorg. Chem.*, 1989, **28**, 2271.
78 P. Chen, E. Danielson and T. J. Meyer, *J. Phys. Chem.*, 1988, **92**, 3708.
79 J. R. Schoonover, P. Chen, W. D. Bates, R. B. Dyer and T. J. Meyer, *Inorg. Chem.*, 1994, **33**, 793.
80 B. D. Rossenaar, D. J. Stufkens and A. Vlček, Jr., *Inorg. Chim. Acta*, 1996, **247**, 247.
81 A. Ponce, H. B. Gray and J. R. Winkler, *J. Am. Chem. Soc.*, 2000, **122**, 8187.
82 W. D. Bates, P. Chen, C. A. Bignozzi, J. R. Schoonover and T. J. Meyer, *Inorg. Chem.*, 1995, **34**, 6215.
83 D. R. Gamelin, M. W. George, P. Glyn, F.-W. Grevels, F. P. A. Johnson, W. Klotzbucher, S. L. Morrison, G. Russell, K. Schaffner and J. J. Turner, *Inorg. Chem.*, 1994, **33**, 3246.